

Equilibrium physics breakdown reveals the active nature of red blood cell flickering

H. Turlier^{1,2,3}, D. A. Fedosov⁴, B. Audoly^{3,5}, T. Auth⁴, N. S. Gov⁶, C. Sykes², J.-F. Joanny^{2,3,7}, G. Gompper⁴ and T. Betz^{2,8*}

Red blood cells, or erythrocytes, are seen to flicker under optical microscopy, a phenomenon initially described as thermal fluctuations of the cell membrane. But recent studies have suggested the involvement of non-equilibrium processes, without definitively ruling out equilibrium interpretations. Using active and passive microrheology to directly compare the membrane response and fluctuations on single erythrocytes, we report here a violation of the fluctuation-dissipation relation, which is a direct demonstration of the non-equilibrium nature of flickering. With an analytical model of the composite erythrocyte membrane and realistic stochastic simulations, we show that several molecular mechanisms may explain the active fluctuations, and we predict their kinetics. We demonstrate that tangential metabolic activity in the network formed by spectrin, a cytoskeletal protein, can generate curvature-mediated active membrane motions. We also show that other active membrane processes represented by direct normal force dipoles may explain the observed membrane activity. Our findings provide solid experimental and theoretical frameworks for future investigations of the origin and function of active motion in cells.

One of the first observations of red blood cells (RBC) by optical microscopy during the nineteenth century was the ‘vibrating’ fluctuation of its plasma membrane¹. Important biological functions of this flickering have been suggested, such as decreased interactions between cells² or facilitated diffusion of membrane proteins³. Today, flickering analysis is envisaged as a promising tool for high-rate malaria diagnosis⁴. However, although equilibrium fluctuation models^{5–7} have been used to infer mechanical properties of RBCs since the seminal work of Brochard and Lennon⁸, the fundamental question whether membrane fluctuations are driven by an active process or simply by thermal agitation remains controversial^{9–12}.

Possible active metabolic origins were conjectured more than 60 years ago¹³, but were readily questioned by the observation that flickering arises in reconstituted membranes as well. By comparing membrane fluctuations directly between healthy RBCs and cells depleted of ATP (adenosine triphosphate), recent experiments find a decrease of fluctuations on ATP-depletion, hence suggesting that an active process may contribute to membrane undulations^{6,14–16}. However, the passive mechanical properties of the RBC membrane themselves depend strongly on ATP, as illustrated by the stiffening of the RBC membrane on starvation^{6,15,17–19}, which correlates with a sudden transition from discocyte to spiculated echinocyte shapes^{20,21}. Therefore, a direct and compelling explanation for the decrease of fluctuations observed in ATP-depleted cells is the stiffening of the membrane^{22,23} rather than the loss of putative active (that is, non-equilibrium) fluctuations. To make a different assessment of the involvement of metabolic activity in flickering, an attractive approach was used by Tuvia *et al.*¹⁴: at equilibrium, the mean-square fluctuations amplitude is a thermodynamic variable,

which, by definition, cannot depend on the dynamics, and in particular on medium viscosity. Tuvia *et al.*¹⁴ reported a viscosity dependence of the mean-square fluctuations amplitude in the frequency range 0.3–30 Hz on changing the suspending medium, and therefore drew the conclusion of a metabolic origin of the flickering. However, recent analysis of fluctuations over a larger bandwidth (0.1–1,000 Hz) shows no detectable dependence of fluctuation amplitudes on medium viscosity⁶, as also confirmed here (Supplementary Fig. 1 and Supplementary Information Appendix C), hence making the conclusions of Tuvia *et al.* equivocal. Recent publications^{15,24} reported non-Gaussian features in the RBC membrane fluctuations distribution and associated them with an active mechanism. However, an equilibrium fluctuations distribution is also likely to exhibit non-Gaussian tails, as soon as anharmonicities are present in the membrane^{25,26}. On the other hand, the fluctuations distribution of a non-equilibrium system can be perfectly Gaussian^{25,27}. As a consequence, the observation of Gaussian fluctuations distributions^{6,9,11,12} does not necessarily imply that RBC flickering is purely thermal. ATP-dependent temporal correlations, consistent with an active component, were recently identified¹⁶; however, their interpretation is model-dependent and does not provide unequivocal evidence for active forces.

An unquestionable hallmark of equilibrium systems is alternatively found in the fluctuation-dissipation theorem (FDT), which relates directly mechanical properties to fluctuations in the linear regime²⁸. By measuring the response function and spontaneous fluctuations for the same system and for the same experimental conditions, it is possible to assert directly the presence of non-equilibrium processes, as recently demonstrated *in vitro* for hair bundles²⁹, active gels³⁰ and suspended bone cells³¹. A series of

¹European Molecular Biology Laboratory, Meyerhofstrasse 1, 69117 Heidelberg, Germany. ²Institut Curie, PSL Research University, CNRS, UMR 168, 75005 Paris, France. ³Sorbonne Universités, UPMC Université Paris 06, 4 place Jussieu, 75005 Paris, France. ⁴Institute of Complex Systems and Institute for Advanced Simulation (ICS-2/IAS-2), Forschungszentrum Jülich, 52425 Jülich, Germany. ⁵CNRS, Institut Jean Le Rond d'Alembert UMR7190, 4 place Jussieu, 75005 Paris, France. ⁶Department of Chemical Physics, Weizmann Institute of Science, 76100 Rehovot, Israel. ⁷ESPCI-ParisTech, 10 rue Vauquelin, 75005 Paris, France. ⁸Institute of Cell Biology, Center for Molecular Biology of Inflammation, Cells-in-Motion Cluster of Excellence, Münster University, Von-Esmarch-Strasse 56, D-48149 Münster, Germany. *e-mail: timo.betz@uni-muenster.de

techniques allow the measurement of cellular mechanics³², and the RBC membrane response has been measured previously using micropipette aspiration³³, electric fields³⁴, or optical tweezers^{10,35}, but never compared directly to the fluctuations in the same cell. Here, we use active and passive microrheology to measure directly single erythrocyte membrane response and fluctuations for the same cell over timescales from milliseconds up to tens of seconds, a range which remains unattained so far¹⁰.

The experimental approach relies on a time-shared multiplexed optical tweezer, generating four independent traps that control the position of four streptavidin-functionalized polystyrene beads attached to a biotinylated RBC at opposite sites along its rim (Fig. 1 and Supplementary Fig. 2). The beads allow us to apply well-defined forces on the cell membrane, but they can also track local membrane shape deformation with sub-nm accuracy and avoid problems related to the convolution between the cell edge and the detection laser when directly tracking the membrane^{6,36}. Using this set-up we can detect both the free fluctuations and mechanical response of the cell membrane with sub-millisecond temporal resolution, thanks to an interferometric detection system (Fig. 1a). Three beads (Fig. 1a inset) serve as handles to hold the cell 20 μm above the coverslip surface in the observation chamber. The fourth bead is used as a probe (Fig. 1a inset) to detect free fluctuations or to measure the mechanical response of the membrane under external driving.

In a first experimental step, the free membrane fluctuations are determined by reducing the laser trap power on the probe bead from 5 mW to 0.1 mW. This value is insufficient for stable trapping, but does allow laser-tracking of the bead position. We checked carefully that the presence of this weak trap does not restrict the fluctuations (Supplementary Fig. 3). Therefore, the bead motion directly reflects membrane fluctuations (Fig. 1b), which are characterized by their power spectrum density (PSD) $C(f)$, expressed as function of the frequency f . Furthermore, the influence of the bead on the PSD remains lower than measurement error in the frequency range probed here when compared to the free membrane (Supplementary Fig. 4). Immediately after PSD measurement, the mechanical response is determined for the same cell in a second experiment, where the three handle traps remain unchanged but the average laser power on the probe bead is increased to 5 mW. Sinusoidal oscillations of the probe trap at a driving frequency f (Fig. 1c, blue) displace it over a 200 nm amplitude (Fig. 1c, green). The complex response function $\chi(f)$ is calculated as the ratio between the Fourier transforms of the position $x(f)$ and force $F(f)$ at the driving frequency f . The real and imaginary parts of the response function, χ' and χ'' , correspond respectively to the elastic and the dissipative components of the linear response of the RBC membrane to the applied force. To obtain the frequency-dependent response function, we repeat this active rheology measurement for driving frequencies ranging from 0.2 Hz to 1 kHz. We check the linearity of the response by investigating the force–deformation relation as well as the absence of higher harmonics in the bead displacement and response spectra for each driving force (Supplementary Fig. 5). For both active and passive microrheology measurements, the handle beads move around their equilibrium position. Hence, the probe-bead movement combines the mechanics of the cell and the handle traps. Fluctuations and mechanical response functions are measured under the exact same experimental conditions, which enables us to directly test the validity of the FDT (ref. 28), which reads

$$C(f) = 2k_B T \chi''(f)/(2\pi f) \quad (1)$$

where $k_B T$ is the thermal energy, with k_B being Boltzmann's constant.

We check for violation of the FDT in fresh RBCs, as well as in cells that were ATP-depleted by incubation in glucose-free medium (GFM) at 37 °C for 16 h (partial ATP-depletion) and >48 h (full

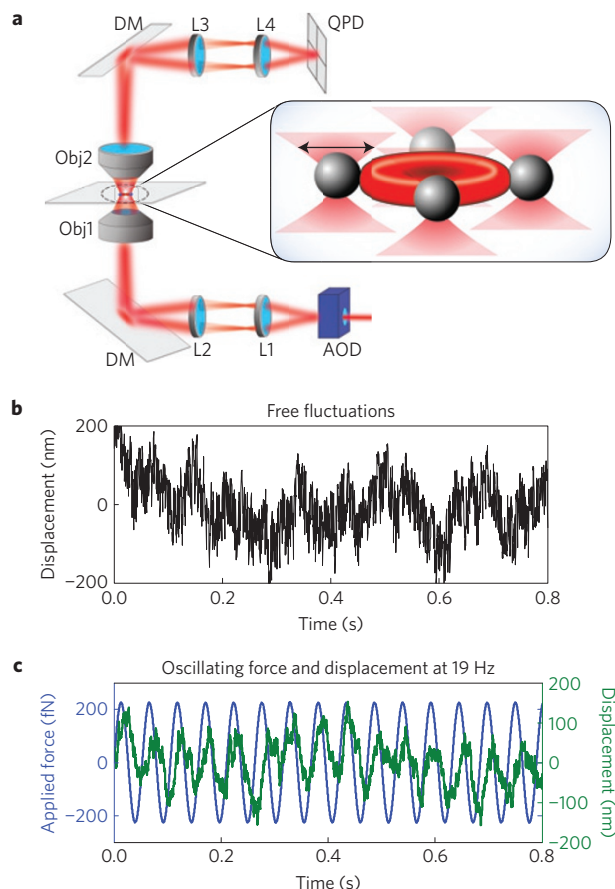


Figure 1 | Experimental set-up. **a**, The position of an infrared laser is controlled by a pair of acousto-optical-deflectors (AOD) that allow rapid beam scanning (6 μs switching time). The beam is relayed by a telescope to enter the back focal plane of a $\times 60$ NA 1.2 water immersion objective (Obj1), and focused into the sample chamber. The light is collected using a $\times 60$ NA 0.9 water immersion objective (Obj2), and the back focal plane of this objective is imaged onto a quadrant photodiode (QPD). Four beads are attached to the RBC, as sketched in the inset. One bead (marked by black arrow) is used as probe bead either to detect fluctuations or is moved by a sinusoidal force. **b**, Typical time record of the membrane fluctuations. **c**, Typical time record of the membrane response (green) to a sinusoidal force at 19 Hz (blue). The phase shift of about 20 ms is due to dissipation.

ATP-depletion). For fully ATP-depleted cells (nine experiments on seven cells) Fig. 2a plots the dissipative part of the response function and the predictions from the FDT based on the PSD measurements (equation (1)). The observed collapse of both data sets demonstrates the validity of the FDT for a purely passive RBC, as expected. In strong contrast, fresh RBCs (21 experiments on 9 cells) show a clear violation of the FDT in the low-frequency regime $f < 10$ Hz (Fig. 2b). This result is a direct and conclusive demonstration that an active mechanical process contributes to the flickering of the RBC membrane at timescales above 100 ms. Conversely, the collapse of free fluctuations and response at high frequencies ($f > 10$ Hz) indicates the validity of the FDT for rapid fluctuations. Therefore, thermal agitation is the dominant source of fluctuations at short timescales (<100 ms). We conclude that fluctuation measurements can be reliably used to infer mechanical properties of the RBC membrane only in this high-frequency limit. The validity of previous studies, which used equilibrium theories to extract mechanical information on the RBC membrane, has therefore to be critically checked. The comparison of the dissipative response for the three conditions (zero, partial and full ATP-depletion) in Fig. 2c

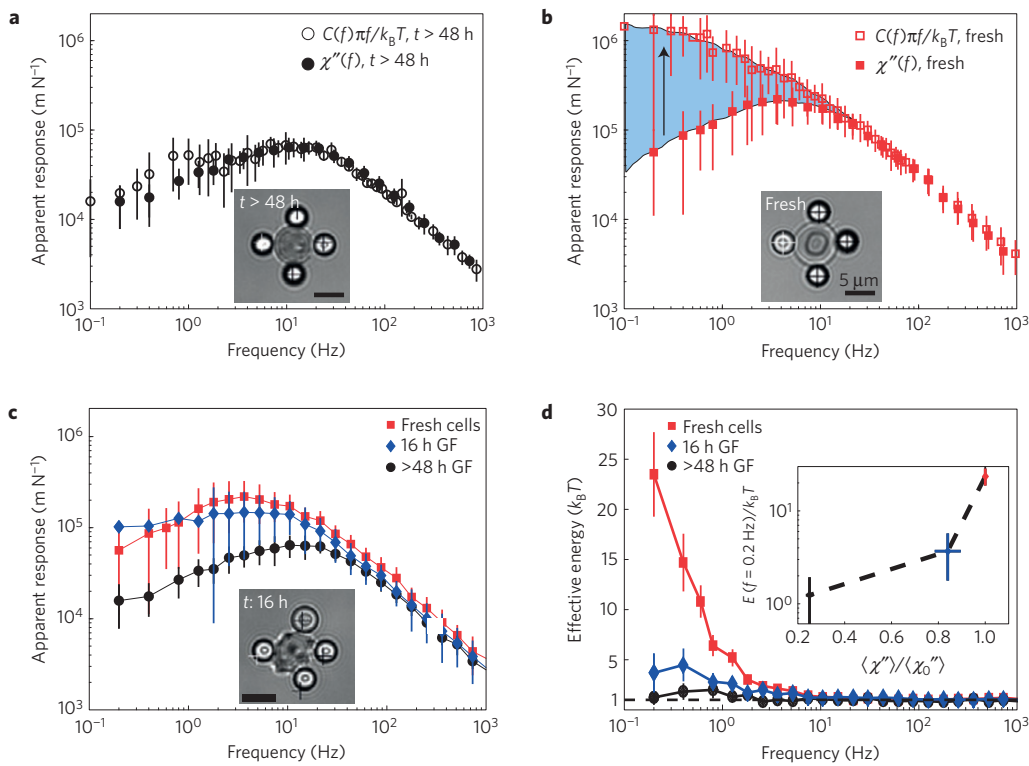


Figure 2 | Membrane fluctuations and apparent response. **a**, After 48 h incubation in glucose-free medium (GFM) at 37 °C, the measured response function (filled black circles) coincides with the response calculated from the power spectrum density $C(f)$ measurement (open black circles) using the fluctuation-dissipation theorem (equation (1)). (Inset) RBC after >48 h in GFM. **b**, For fresh RBCs, the measured response (filled red squares) and the response calculated from fluctuations measurement (open red squares) differ below 10 Hz by more than an order of magnitude, indicating a clear violation of the FDT. **c**, The dissipative response is moderately reduced for 16 h GFM, and strongly reduced for >48 h GFM. (Inset) RBC after >16 h in GFM. **d**, Effective energy $E_{\text{eff}}(f) = C(f)\pi f/\chi''(f)$ for fresh RBCs (red), after 16 h in GFM (blue) and for >48 h in GFM (black). (Inset) Low-frequency (0.2 Hz) effective energy as a function of relative mechanical changes. Error bars denote s.d. Scale bars are 5 μm.

confirms the strong metabolic dependence of passive membrane properties noted previously^{6,12,18,22,23}.

To measure directly the metabolic energy input which drives active fluctuations, we use the concept of effective energy⁶ $E_{\text{eff}}(f)$, defined as the thermal energy at a frequency f that would be necessary to recover the FDT in the non-equilibrium system, given by $E_{\text{eff}}(f) = C(f)\pi f/\chi''(f)$. The metabolic energy input driving active flickering is visualized directly above $1k_B T$ in Fig. 2d. Interestingly, ATP-depletion of RBCs is not fully complete after 16 h of incubation in glucose-free medium^{17,37}. The effective energy coincides with the thermal energy at high frequency for all conditions, but it increases up to $23k_B T$ at low frequencies for fresh RBCs (ref. 27). Integrating this deviation over the full spectrum gives an estimate of the power $P_f \sim 0.025 \text{ fW}$ used for driving the membrane fluctuations. This is only a very small fraction of the total metabolic energy turnover in the RBC (ref. 38) of $P_{\text{RBC}} \sim 10 \text{ fW}$.

Diverse metabolic processes have been identified in the RBC membrane. We use here analytical and simulation models to explore their relevance in explaining the observed active fluctuations. The membrane consists of a network of spectrin filaments anchored to a lipid bilayer, as illustrated in Fig. 3a. Biochemists identified several phosphorylation sites directly in the network: at the transmembrane protein complexes 4.1R (refs 23,39,40) and ankyrin⁴¹, which anchor the network in the bilayer, but also at the spectrin chains²². These phosphorylations have been associated with a decreased mechanical strength of the membrane^{6,15,22,23,42}, but the underlying molecular mechanism remains unclear. Instead of considering one specific process, we argue here that any relevant spectrin phosphorylation should lead to a local decrease of the network shear modulus, as this single parameter characterizes its mechanical properties. Our

mean-field approach therefore encompasses the filament detachment hypothesis^{42,43}, but also other potential spectrin metabolic processes. More precisely, we assume a simple two-state dynamics, where phosphorylation sites can switch between active and inactive states with transition rates k_a and k_i respectively, hence defining a mean activity $\langle n_a \rangle = k_a/(k_a + k_i)$. The network shear modulus fluctuates accordingly around a mean value, $\langle \mu \rangle = \mu_0(1 - \langle n_a \rangle)$, that decreases with phosphorylation. Modelling the RBC membrane mechanics remains a challenging task, as multiple length scales and timescales are involved. Most previous composite models are hence numerical^{44–47} or limited to flat geometries^{16,42,43,48–50}. We derive here an active composite membrane model in a spherical geometry, while considering explicitly the finite elasticity of the spectrin network and its sliding relative to the bilayer.

The spectrin cytoskeleton is idealized as a perfect triangular network of springs. In line with previous studies^{33,42,51}, we assume it to be prestressed (see Fig. 3a). The filaments are homogeneously prestretched by a factor $\xi > 1$, which preserves the six-fold symmetry of the network⁵². We can hence homogenize the discrete filament energy into an effectively isotropic continuous elastic membrane that we describe in the regime of finite elasticity (see Supplementary Information p13–16). Its energy, expressed as a function of the incremental deformations from the prestressed state, is Hookean and includes a prestress term. Integrated over the membrane surface A , it reads $E = \int dA [\varepsilon_i + S e_{\alpha\alpha} + M((1/2)(e_{\alpha\beta})^2 + e_{\alpha\beta}^2)]$, where ε_i is the constant energy density due to prestress and $e_{\alpha\beta}$ is the nonlinear incremental membrane strain tensor. The prestressed network mechanics is characterized by an effective spectrin tension S and an incremental shear modulus M , which are both functions of the prestretch ratio ξ , the phosphorylation activity $\langle n_a \rangle$ and the

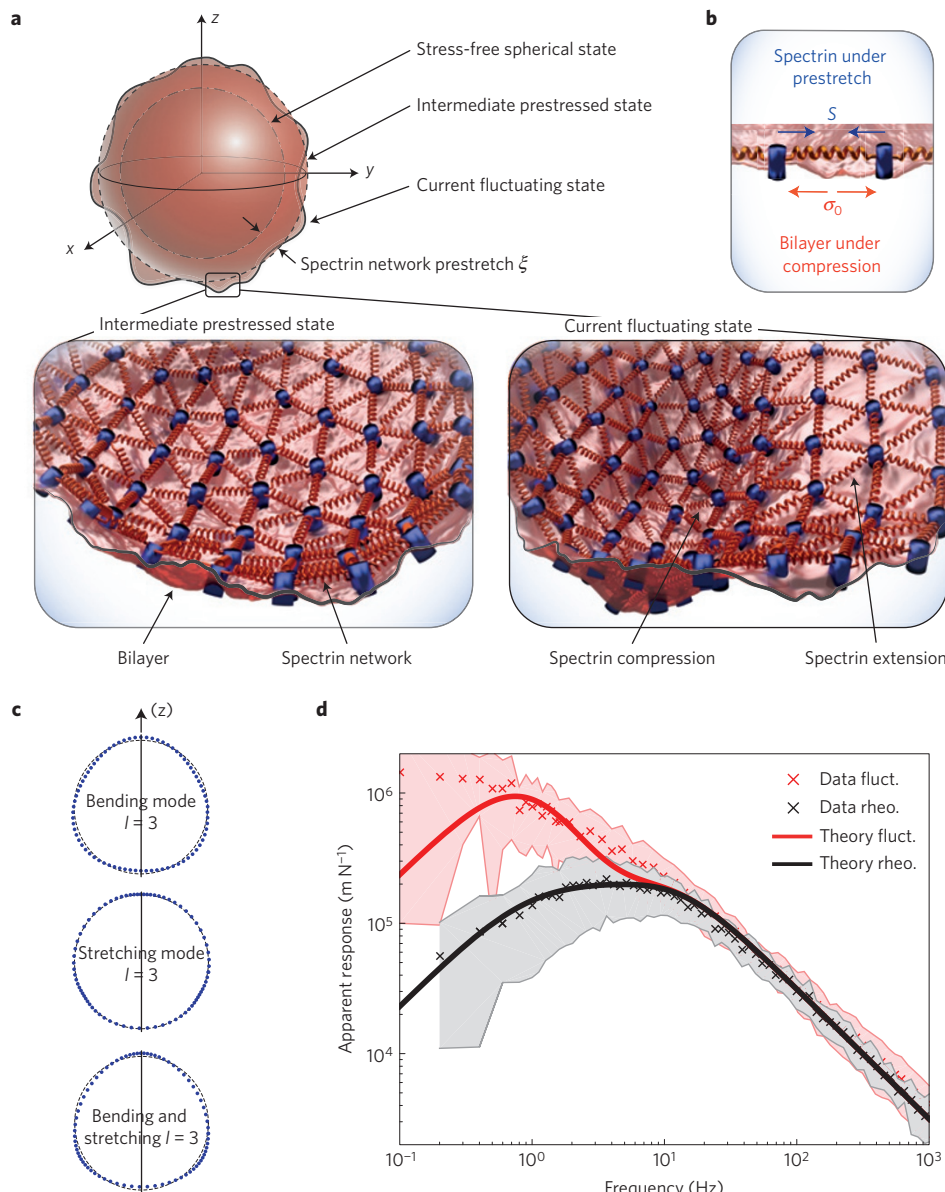


Figure 3 | Analytic composite model of the red blood cell membrane. **a**, Schematic description of the membrane geometry and configurations: the membrane is composed of the lipid bilayer and a regular triangular network of spring-like spectrin filaments. It fluctuates around an intermediate state where the spectrin network is prestressed and the bilayer compressed on average. **b**, A large enough excess area of lipid bilayer creates a negative bilayer tension σ_0 , as a result of its tangential compression. This bilayer elastic contribution can counterbalance the effective spectrin tension S , which results from filament prestretch. **c**, The membrane deformation is a combination of bending and stretching modes, illustrated here for the spherical harmonic $l=3$. **d**, The analytic model (solid lines) can reproduce the experimental fluctuations and response data (crosses). Shaded areas denote s.d.

stress-free shear modulus μ_0 . For vanishing prestress ($\xi = 1$) the spectrin tension vanishes and $M = \langle \mu \rangle$ (Supplementary Fig. 6). Extending a previous approach⁵³, we derive the elastic forces of the spectrin network and expand them into vector spherical harmonics, which allows one to identify the three elementary modes of deformation: bending, stretching and shear. As usual in thin-shell theory, bending and stretching deformations are linearly coupled for curved membranes, as illustrated in Fig. 3c for the harmonic $l = 3$; by contrast, shear is decoupled here and is therefore ignored. The inextensible lipid bilayer is classically characterized by a bending modulus κ and a surface tension σ_0 , and its elastic forces can be derived from the Canham–Helfrich energy^{54,55} $H = \int (\kappa/2C^2 + \sigma_0) dA$, where C measures the mean local curvature.

The dissipative forces on the membrane have several sources. The inner and outer fluids have different viscosities and exert

viscous stresses⁵³, whereas the relative movement of the spectrin with respect to the lipid bilayer leads to a tangential friction force. Surprisingly, this friction force is found to largely overcome viscous damping for large wavelengths; it therefore controls the tangential relaxation dynamics (Supplementary Fig. 6). A Langevin membrane dynamics is obtained by combining elastic and dissipative forces with thermal noise. This leads, for a given spherical harmonic (l, m) , to an effective dynamics coupling bending $u_{lm}^{(r)}$ and stretching $u_{lm}^{(1)}$ deformations

$$\frac{d\mathbf{U}_{lm}(t)}{dt} = -W_{lm} \times \mathbf{U}_{lm}(t) + \mathbf{Z}_{lm}^{TH}(t) + \mathbf{Z}_{lm}^A(t) \quad (2)$$

where W_{lm} is the relaxation frequency matrix for the membrane deformation $\mathbf{U}_{lm} = (u_{lm}^{(r)}, u_{lm}^{(1)})$. The thermal noise $\mathbf{Z}_{lm}^{TH}(t)$ naturally

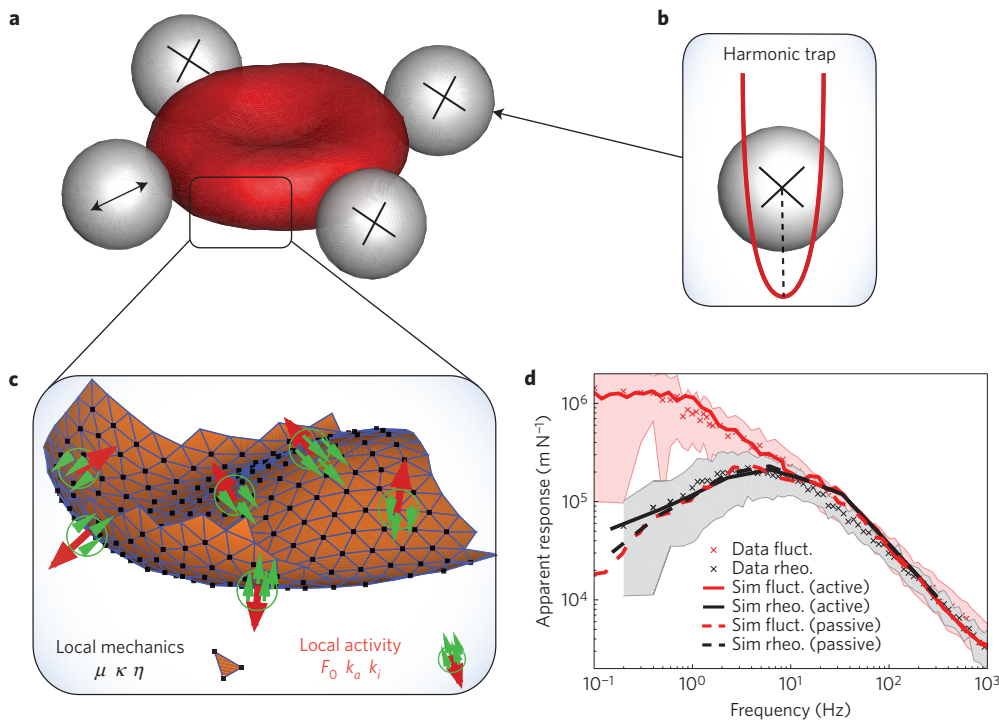


Figure 4 | Simulations mimicking the experimental conditions. **a**, Simulation set-up with a RBC and four beads attached. Three beads (marked by crosses) are used as handles via a harmonic potential, whereas the fourth probe bead (marked by a two-headed arrow) is either sinusoidally driven to measure the mechanical response or left free to monitor its fluctuations. **b**, Illustration of a bead whose centre-of-mass is held in a harmonic potential. The harmonic potential mimics the optical tweezer trap in experiments and assumes the same strength for this trap. **c**, Close-up of the membrane illustrating the coarse-grained membrane network structure and the forces applied to mimic activity of a RBC. The local membrane mechanics includes shear and bending moduli μ and κ , respectively, and surrounding fluids of viscosity η . The active forces at the membrane (indicated by red arrows) of amplitude F_0 are applied in the normal direction with equal probability inwards and outwards with respect to the membrane. Their kinetics is characterized by active and inactive transition rates k_i and k_a . The green arrows correspond to the counteracting forces applied locally to the surrounding fluids representing force dipoles. **d**, Comparison of the simulation results with the experimental measurements. Simulations with force dipoles (active) reproduce experimental measurements of the response (rheo.) and fluctuations (fluct.) well. When activity is turned off (passive), the FDT is recovered as in fully ATP-depleted RBCs (Fig. 2a). Shaded areas denote s.d.

contributes to both bending and stretching fluctuations, whereas metabolic shear modulus fluctuations $\mu_{lm}(t)$ in an isolated network generate direct active forces both in the tangential and normal directions. When the network is coupled to the bilayer, however, we predict the local bilayer incompressibility to systematically cancel the direct active normal force and we end up with an additional active source of noise for the stretching modes only, $Z_{lm}^A(t) = (0, \Omega_{lm}^A \mu_{lm}(t))$. This is, therefore, in contrast to previous phenomenological active models based on the existence of a direct active normal force^{16,42}. Tangential metabolic noise nevertheless perturbs normal membrane motions via the curvature-mediated coupling between bending and stretching modes (non-diagonal components of the matrix W_{lm}). This effect is dampened by the friction between the bilayer and the network, and therefore depends critically on the tangentially fluid character of the bilayer. The membrane shape fluctuation spectrum for each spherical harmonic (l, m) can be calculated in Fourier space as a sum over the dissipative part of the response function $\chi''_{lm}(f)$ and this active contribution

$$C_{lm}(f) = \frac{2k_B T}{2\pi f} \chi''_{lm}(f) + \frac{2\langle n_a \rangle (1 - \langle n_a \rangle) \tau_a}{1 + (2\pi f \tau_a)} |N_{lm}(f)|^2 \quad (3)$$

where $N_{lm}(f)$ captures the complex mode- and frequency-dependent propagation of tangential active noise into membrane shape fluctuations. The deviation from FDT is characterized by an active timescale $\tau_a = (k_a + k_i)^{-1}$, which controls the frequency below which a departure from equilibrium is observed for a specific mode

(l, m) : for active timescales much lower than the typical membrane relaxation frequency $|W_{lm}|$, the membrane does not have time to move and the metabolic activity is ineffective, whereas for larger active timescales the FDT violation increases and finally saturates at a value set by the maximum energy input in the system (see Supplementary Fig. 6). We calculate the fluctuation spectrum $C(f)$ as a sum over the relevant modes ($l \geq 2, -l \leq m \leq l$) and predict a violation of FDT for non-zero metabolic activity $\langle n_a \rangle (1 - \langle n_a \rangle) > 0$ and for a prestressed spectrin network $\xi > 1 \Leftrightarrow S > 0$, in agreement with previous hypotheses^{42,43}. In contrast, we find here that the violation vanishes for flat membranes ($R \rightarrow \infty$). The membrane curvature is therefore a key feature for propagating tangential spectrin activity into normal shape motions, and we predict an increase of active fluctuations with membrane curvature, which may explain the higher fluctuations recently measured along the rim of the RBC compared to its central region^{15,24}. To fit the experimental data for rheological tests we use typical mechanical parameters for the RBC that have been either experimentally measured or estimated in simulations, and four fitting parameters (see Supplementary Table): the active rates $k_a = 1.12 \text{ s}^{-1}$ and $k_i = 5.6 \text{ s}^{-1}$, leading to a mean fraction of active sites $\langle n_a \rangle \approx 17\%$, the network prestretch $\xi = 1.04$, controlling both passive and active spectrin mechanics, and the lipid bilayer excess area $\Delta \approx 1.9\%$, which determines the bilayer tension^{56,57} (see Supplementary Information p29–31). Our model shows excellent agreement with the passive response of the membrane and can reproduce the active fluctuation spectrum (Fig. 3d). A broader distribution of active

timescales may refine this agreement and could arise from a Bell-like dependence of the transition rates on membrane extension⁵⁸. Interestingly, we find a slightly negative lipid bilayer tension $\sigma_0 = -6.5 \times 10^{-7} \text{ J m}^{-2}$, which reveals a tangential compression of the bilayer, in agreement with a previous independent estimation⁴⁸. Writing the force balance for the harmonic $l=0$, which reduces to the Laplace law $\Delta P = 2(S + \sigma_0)/R$, we find that the elastic contribution arising from compression of the bilayer is large enough to counterbalance intrinsically the spectrin tension $S > 0$ in the membrane, even in the absence of a pressure jump (Fig. 3b). Our analytical model is therefore self-consistent and shows that the composite nature of the RBC membrane allows it to maintain an intrinsic prestress, a necessary feature for the emergence of spectrin-based active fluctuations.

To investigate the role of other potential metabolic processes in flickering, such as ion pumps⁵⁹ or phospholipid translocase⁶⁰ activities, we employ a cell-scale *in-silico* model, which allows us to closely mimic the experimental situation, including the biconcave RBC geometry, the membrane curvature and stretching elasticity, the attached beads, and the optical tweezers. In our simulations, the hydrodynamics of the internal and external fluids and thermal fluctuations are taken into account by a particle-based mesoscale simulation technique, the dissipative particle dynamics method^{61,62}. Our RBC model (Fig. 4a) is based on a two-dimensional triangulation of the composite membrane⁶³, which corresponds to a network of viscoelastic springs with the inclusion of membrane bending energy and constraints for the conservation of membrane area and volume (see Supplementary Note, Section 1). The spring elements mimic the stretching elasticity of the spectrin network, and simultaneously capture viscous dissipation within the membrane. The bending energy describes bending resistance of the lipid bilayer, whereas the area and volume conservation constraints mimic the incompressibility of the lipid bilayer and cytosol, respectively. Modelling the RBC membrane at the spectrin level is still very challenging for realistic physical conditions (that is, appropriate ambient temperature, membrane elasticity, and long times). To obtain an accurate averaging of fluctuations at the timescales of several minutes, which is much longer than a typical RBC relaxation time, we need to employ a coarse-grained model of the membrane, restricting its triangulation to about a thousand vertices. This coarse-grained description for a RBC has proved to reproduce quantitatively and accurately the viscoelasticity of the RBC membrane, as well as deformation of RBCs due to external forces (laser tweezers) and under flow^{63,64}.

To simulate active processes, we furthermore add random active forces acting normally on membrane vertices (Fig. 4c). For ion pumps, or other membrane protein activity, the force exerted by an active centre has to be counteracted by an exact opposite force in the surrounding fluid. The force density field of active centres therefore has a zero monopole moment, and the first contribution expected is a force dipole⁶⁵.

As in experiments, the three handle beads in simulations are held by a harmonic potential mimicking optical tweezers, whereas the probe bead is moved sinusoidally to determine the mechanical response function (Fig. 4a,b). The free fluctuations of the probe bead are measured in a separate simulation. The simulations reproduce accurately the experimental response function (Fig. 4d), and lead to estimation of the mechanical properties of RBCs (Supplementary Table). The mechanical properties found are fully consistent with previous experimental estimations. Simulations reproduce the experimental violation of the FDT very precisely with the force amplitude $F_0 = 650 \text{ fN}$ for active dipoles and with the transition rates $k_a = 0.42 \text{ s}^{-1}$ and $k_i = 1.3 \text{ s}^{-1}$ between active and inactive states (Fig. 4d). The order of magnitude of the dipole force amplitude is consistent with simple estimates proposed for ion pumps⁶⁵. The timescales are longer than those predicted analytically

with the spectrin activity hypothesis, a difference which may be explained by the large bilayer friction, dampening the propagation of tangential spectrin activity into normal membrane shape fluctuations. When active processes are turned off, the simulated membrane fluctuations correspond to the FDT predictions (Fig. 4d, dashed lines), as expected. The resulting stochastic process for the membrane activity leads to an average fraction of active sites (that is, those with the force applied at any moment of time) on a RBC of about 12%. Thus, our RBC simulations show that simple uncorrelated active force dipoles can reproduce experimental results with excellent accuracy. The agreement between experiments and simulation results, using force dipoles, indicates that the spectrin network, as suggested by our and other theoretical models, may not be the only source of activity in the RBC membrane. In particular, the activity of ion pumps in the membrane might offer a compelling explanation for the active flickering we measure here directly^{59,65}. Simulations also allow efficient testing of hypothetical active processes, such as local force monopoles, that may conserve momentum only globally. Such active force centres fit the data equally well, with the same active rates as force dipoles but with tenfold lower force amplitudes $F_0 = 50 \text{ fN}$, in agreement with previous estimations⁴³ (Supplementary Fig. 7). Therefore, our simulations show that several, non-excluding, underlying mechanisms of uncorrelated active forces may explain membrane activity and suggest that further experimental characterizations are required to clearly identify the molecular mechanisms involved in flickering. They provide clear kinetic and amplitude predictions to guide future experiments.

Methods

Methods and any associated references are available in the [online version of the paper](#).

Received 7 November 2015; accepted 30 November 2015;
published online 18 January 2016

References

1. Browicz, T. Further observation of motion phenomena on red blood cells in pathological states. *Zbl Med. Wiss.* **28**, 625–627 (1890).
2. Evans, E. A. & Parsegian, V. A. Thermal-mechanical fluctuations enhance repulsion between bimolecular layers. *Proc. Natl Acad. Sci. USA* **83**, 7132–7136 (1986).
3. Lin, L. C.-L. & Brown, F. L. H. Dynamics of pinned membranes with application to protein diffusion on the surface of red blood cells. *Biophys. J.* **86**, 764–780 (2004).
4. Cojoc, D. *et al.* Toward fast malaria detection by secondary speckle sensing microscopy. *Biomed. Opt. Express* **3**, 991–1005 (2012).
5. Strey, H., Peterson, M. & Sackmann, E. Measurement of erythrocyte membrane elasticity by flicker eigenmode decomposition. *Biophys. J.* **69**, 478–488 (1995).
6. Betz, T., Lenz, M., Joanny, J.-F. & Sykes, C. ATP-dependent mechanics of red blood cells. *Proc. Natl Acad. Sci. USA* **106**, 15320–15325 (2009).
7. Yoon, Y.-Z. *et al.* Flickering analysis of erythrocyte mechanical properties: dependence on oxygenation level, cell shape, and hydration level. *Biophys. J.* **97**, 1606–1615 (2009).
8. Brochard, F. & Lennon, J. F. Frequency spectrum of the flicker phenomenon in erythrocytes. *J. Phys.* **36**, 1035–1047 (1975).
9. Evans, J., Gratzer, W., Mohandas, N., Parker, K. & Sleep, J. Fluctuations of the red blood cell membrane: relation to mechanical properties and lack of ATP dependence. *Biophys. J.* **94**, 4134–4144 (2008).
10. Yoon, Y. Z., Kotar, J., Brown, A. T. & Cicuta, P. Red blood cell dynamics: from spontaneous fluctuations to non-linear response. *Soft Matter* **7**, 2042–2051 (2011).
11. Boss, D. *et al.* Spatially-resolved eigenmode decomposition of red blood cells membrane fluctuations questions the role of ATP in flickering. *PLoS ONE* **7**, e40667 (2012).
12. Puckeridge, M., Chapman, B. E., Conigrave, A. D. & Kuchel, P. W. Membrane flickering of the human erythrocyte: physical and chemical effectors. *Eur. Biophys. J.* **43**, 169–177 (2014).
13. Blowers, R., Clarkson, E. M. & Maizels, M. Flicker phenomenon in human erythrocytes. *J. Physiol.* **113**, 228–239 (1951).

14. Tuvia, S. *et al.* Cell membrane fluctuations are regulated by medium macroviscosity: evidence for a metabolic driving force. *Proc. Natl Acad. Sci. USA* **94**, 5045–5049 (1997).
15. Park, Y. *et al.* Metabolic remodeling of the human red blood cell membrane. *Proc. Natl Acad. Sci. USA* **107**, 1289–1294 (2010).
16. Rodríguez-García, R. *et al.* Direct cytoskeleton forces cause membrane softening in red blood cells. *Biophys. J.* **108**, 2794–2806 (2015).
17. Weed, R. I., LaCelle, P. L. & Merrill, E. W. Metabolic dependence of red cell deformability. *J. Clin. Invest.* **48**, 795–809 (1969).
18. Chabanel, A., Reinhart, W. & Chien, S. Increased resistance to membrane deformation of shape-transformed human red blood cells. *Blood* **69**, 739–743 (1987).
19. Discher, D. E., Mohandas, N. & Evans, E. A. Molecular maps of red cell deformation: hidden elasticity and *in situ* connectivity. *Science* **266**, 1032–1035 (1994).
20. Nakao, M., Nakao, T. & Yamazoe, S. Adenosine triphosphate and maintenance of shape of the human red cells. *Nature* **187**, 945–946 (1960).
21. Sheetz, M. P. On the mechanism of ATP-induced shape changes in human erythrocyte membranes. I. The role of the spectrin complex. *J. Cell Biol.* **73**, 638–646 (1977).
22. Manno, S., Takakuwa, Y., Nagao, K. & Mohandas, N. Modulation of erythrocyte membrane mechanical function by beta-spectrin phosphorylation and dephosphorylation. *J. Biol. Chem.* **270**, 5659–5665 (1995).
23. Manno, S., Takakuwa, Y. & Mohandas, N. Modulation of erythrocyte membrane mechanical function by protein 4.1 phosphorylation. *J. Biol. Chem.* **280**, 7581–7587 (2005).
24. Monzel, C. *et al.* Measuring fast stochastic displacements of bio-membranes with dynamic optical displacement spectroscopy. *Nature Commun.* **6**, 8162 (2015).
25. Van Kampen, N. G. *Fluctuation Phenomena in Solids* (Academic Press, 1965).
26. Schmidt, D. *et al.* Signature of a nonharmonic potential as revealed from a consistent shape and fluctuation analysis of an adherent membrane. *Phys. Rev. X* **4**, 021023 (2014).
27. Ben-Isaac, E. *et al.* Effective temperature of red-blood-cell membrane fluctuations. *Phys. Rev. Lett.* **106**, 238103 (2011).
28. Callen, H. B. & Welton, T. A. Irreversibility and generalized noise. *Phys. Rev.* **83**, 34–40 (1951).
29. Martin, P., Hudspeth, A. J. & Julicher, F. Comparison of a hair bundle's spontaneous oscillations with its response to mechanical stimulation reveals the underlying active process. *Proc. Natl Acad. Sci. USA* **98**, 14380–14385 (2001).
30. Mizuno, D., Tardin, C., Schmidt, C. F. & MacKintosh, F. C. Nonequilibrium mechanics of active cytoskeletal networks. *Science* **315**, 370–373 (2007).
31. Mizuno, D., Bacabac, R., Tardin, C., Head, D. & Schmidt, C. F. High-resolution probing of cellular force transmission. *Phys. Rev. Lett.* **102**, 168102 (2009).
32. Hoffman, B. D., Massiera, G., Van Citters, K. M. & Crocker, J. C. The consensus mechanics of cultured mammalian cells. *Proc. Natl Acad. Sci. USA* **103**, 10259–10264 (2006).
33. Discher, D. E., Boal, D. H. & Boey, S. K. Simulations of the erythrocyte cytoskeleton at large deformation. II. Micropipette aspiration. *Biophys. J.* **75**, 1584–1597 (1998).
34. Engelhardt, H., Gaub, H. & Sackmann, E. Viscoelastic properties of erythrocyte membranes in high-frequency electric fields. *Nature* **307**, 378–380 (1984).
35. Lenormand, G., Hénon, S., Richert, A., Siméon, J. & Gallet, F. Direct measurement of the area expansion and shear moduli of the human red blood cell membrane skeleton. *Biophys. J.* **81**, 43–56 (2001).
36. Betz, T. & Sykes, C. Time resolved membrane fluctuation spectroscopy. *Soft Matter* **8**, 5317–5326 (2012).
37. Chu, H. *et al.* Identification of cytoskeletal elements enclosing the ATP pools that fuel human red blood cell membrane cation pumps. *Proc. Natl Acad. Sci. USA* **109**, 12794–12799 (2012).
38. Bandmann, U., Monti, M. & Wadsö, I. Clinical physiology: microcalorimetric measurements of heat production in whole blood and blood cells of normal persons. *Scand. J. Clin. Lab. Invest.* **35**, 121–127 (1975).
39. Subrahmanyam, G., Bertics, P. J. & Anderson, R. A. Phosphorylation of protein 4.1 on tyrosine-418 modulates its function *in vitro*. *Proc. Natl Acad. Sci. USA* **88**, 5222–5226 (1991).
40. Gauthier, E., Guo, X., Mohandas, N. & An, X. Phosphorylation-dependent perturbations of the 4.1R-associated multiprotein complex of the erythrocyte membrane. *Biochemistry* **50**, 4561–4567 (2011).
41. Lu, P. W., Soong, C. J. & Tao, M. Phosphorylation of ankyrin decreases its affinity for spectrin tetramer. *J. Biol. Chem.* **260**, 14958–14964 (1985).
42. Gov, N. S. & Safran, S. A. Red blood cell membrane fluctuations and shape controlled by ATP-induced cytoskeletal defects. *Biophys. J.* **88**, 1859–1874 (2005).
43. Gov, N. S. Active elastic network: cytoskeleton of the red blood cell. *Phys. Rev. E* **75**, 011921 (2007).
44. Boal, D. H., Seifert, U. & Zilker, A. Dual network model for red blood cell membranes. *Phys. Rev. Lett.* **69**, 3405–3408 (1992).
45. Peng, Z., Asaro, R. J. & Zhu, Q. Multiscale modelling of erythrocytes in Stokes flow. *J. Fluid Mech.* **686**, 299–337 (2011).
46. Li, H. & Lykotrafitis, G. Two-component coarse-grained molecular-dynamics model for the human erythrocyte membrane. *Biophys. J.* **102**, 75–84 (2012).
47. Peng, Z. *et al.* Lipid bilayer and cytoskeletal interactions in a red blood cell. *Proc. Natl Acad. Sci. USA* **110**, 13356–13361 (2013).
48. Fournier, J.-B., Lacoste, D. & Raphaël, E. Fluctuation spectrum of fluid membranes coupled to an elastic meshwork: jump of the effective surface tension at the mesh size. *Phys. Rev. Lett.* **92**, 018102 (2004).
49. Dubus, C. & Fournier, J.-B. A Gaussian model for the membrane of red blood cells with cytoskeletal defects. *Europhys. Lett.* **75**, 181–187 (2006).
50. Zhang, R. & Brown, F. L. H. Cytoskeleton mediated effective elastic properties of model red blood cell membranes. *J. Chem. Phys.* **129**, 065101 (2008).
51. Paulose, J., Vliegenthart, G. A., Gompper, G. & Nelson, D. R. Fluctuating shells under pressure. *Proc. Natl Acad. Sci. USA* **109**, 19551–19556 (2012).
52. Kantor, Y. Entropic elasticity of tethered solids. *Phys. Rev. A* **39**, 6582–6586 (1989).
53. Rochal, S. B., Lorman, V. L. & Mennessier, G. Viscoelastic dynamics of spherical composite vesicles. *Phys. Rev. E* **71**, 021905 (2005).
54. Canham, P. B. The minimum energy of bending as a possible explanation of the biconcave shape of the human red blood cell. *J. Theor. Biol.* **26**, 61–81 (1970).
55. Milner, S. T. & Safran, S. A. Dynamical fluctuations of droplet microemulsions and vesicles. *Phys. Rev. A* **36**, 4371–4379 (1987).
56. Seifert, U. The concept of effective tension for fluctuating vesicles. *Z. Phys. B* **97**, 299–309 (1995).
57. Loubet, B., Seifert, U. & Lohmolt, M. A. Effective tension and fluctuations in active membranes. *Phys. Rev. E* **85**, 031913 (2012).
58. Bähr, T., Seifert, U. & Smith, A.-S. Nucleation of ligand-receptor domains in membrane adhesion. *Phys. Rev. Lett.* **109**, 258101 (2012).
59. Prost, J. & Bruinsma, R. Shape fluctuations of active membranes. *Europhys. Lett.* **33**, 321–326 (1996).
60. Graham, T. R. Flippases and vesicle-mediated protein transport. *Trends Cell Biol.* **14**, 670–677 (2004).
61. Hoogerbrugge, P. J. & Koelman, J. M. V. A. Simulating microscopic hydrodynamic phenomena with dissipative particle dynamics. *Europhys. Lett.* **19**, 155–160 (1992).
62. Español, P. & Warren, P. Statistical mechanics of dissipative particle dynamics. *Europhys. Lett.* **30**, 191–196 (1995).
63. Fedosov, D. A., Caswell, B. & Karniadakis, G. E. A multiscale red blood cell model with accurate mechanics, rheology, and dynamics. *Biophys. J.* **98**, 2215–2225 (2010).
64. Fedosov, D. A., Noguchi, H. & Gompper, G. Multiscale modeling of blood flow: from single cells to blood rheology. *Biomech. Model. Mechanobiol.* **13**, 239–258 (2014).
65. Manneville, J.-B., Bassereau, P., Ramaswamy, S. & Prost, J. Active membrane fluctuations studied by micropipet aspiration. *Phys. Rev. E* **64**, 021908 (2001).

Acknowledgements

We thank V. L. Lorman and J. Prost for careful reading of the analytical model. T.B. was founded by ANR-11-JSV5-0002 and by the Deutsche Forschungsgemeinschaft (DFG), Cells-in-Motion Cluster of Excellence (EXC 1003—CiM), University of Münster, Germany. H.T. acknowledges funding from the EMBL Interdisciplinary Postdoc program under Marie Curie Actions FP7-PEOPLE-2011-COFUND and generous support from the Bettencourt Schueller Foundation. D.A.F. acknowledges funding by the Alexander von Humboldt Foundation. D.A.F., T.A. and G.G. gratefully acknowledge a CPU time grant by the Jülich Supercomputing Center. N.S.G. acknowledges the Institut Curie's Mayent-Rothschild Visiting Professor fund and Labex CelTisPhyBio for their support during the stay at the Institut Curie. N.S.G. is the incumbent of the Lee and William Abramowitz Professorial Chair of Biophysics, and thanks ISF Grant 580/12 for support.

Author contributions

T.B. and C.S. designed experiments; T.B. performed experiments; H.T., B.A. and J.-F.J. derived the analytical model; D.A.F., T.A. and G.G. designed the simulation set-up; D.A.F. performed simulations; T.B., H.T. and D.A.F. analysed the data; all authors discussed and interpreted results; all authors wrote the manuscript.

Additional information

Supplementary information is available in the online version of the paper. Reprints and permissions information is available online at www.nature.com/reprints. Correspondence and requests for materials should be addressed to T.B.

Competing financial interests

The authors declare no competing financial interests.

Methods

Experimental preparation and effects on tension. Biotinylated red blood cells are prepared as described previously⁶⁶ and mixed with streptavidin-coated beads (3.28 μm diameter). Four beads are attached to the RBC in an opposing geometry (Fig. 1) by trapping and manipulating the beads and the RBC using the multiplexed optical tweezers. The attachment area of the bead on the membrane was visually estimated to be about 1 μm in diameter (Supplementary Methods and Supplementary Fig. 2), which corresponds to about 2% of the RBC membrane. The resulting increase of tension can be estimated to be only about 0.2%, and will hence not have a significant impact on the membrane fluctuations.

Bead and membrane motions. In the experiments we use the probe bead not only to determine the free fluctuations of the membrane, but also to apply a given force to the cell. The handle beads are exclusively used to keep the system in a stable 3D situation 20 μm above the substrate. To test to what extent the probe-bead fluctuations actually represent the membrane motion we also prepared sample cells with only three handle beads and measured the membrane fluctuations on the position where the fourth bead is usually attached, using the methods reported previously⁶. Supplementary Fig. 4 shows an overlay of the free probe-bead fluctuations and the free membrane. Within the error, the two remain typically equal, and only at low frequencies is there a systematic, but insignificant difference between the probe bead and the membrane. Interestingly, the membrane fluctuations in this 3D situation are a factor of five higher than the fluctuations measured on the sedimented RBC (Supplementary Fig. 4). Hence, when modelling the RBC membrane fluctuations, surface effects such as gravity-mediated interactions as well as friction need to be taken into account for a correct analysis. To this end, our results can explain the previously found overestimation of RBC viscosities in the fluctuation analysis of sedimented cells⁶.

Effect of the trapping laser on measurements. To verify that the weak laser does not suppress any fluctuations, we compare the PSD of a free bead to the PSD of a bead attached to the RBC in the experimental situation described, using 0.1 mW in both cases. The resulting plot (Supplementary Fig. 3) shows that the motion of the bead is indeed limited by the cell, as the free bead fluctuations are larger over the full frequency range.

Furthermore, we checked that the response function measured by the active microrheology does not simply reflect the trap stiffness of the handle beads. This was verified by comparing the PSD of the handle beads with the PSD derived from the measured response function (Supplementary Fig. 8). The result shows that the response function of the cell is different from the response function imposed by the handle traps over the relevant frequency regime of 0.1–100 Hz. Hence, the response function does indeed reflect the RBC mechanics.

Possible heating effects of the laser on the cell cannot be excluded. We can see haemolysis of cells if trapped with 100 mW for more than 30 min. However, with the applied laser intensities we do not observe any effect during the experiments. As both the active and passive measurements are done in the same situation (handle beads trapped with 5 mW), the typical heating should be similar in both situations and not lead to a systematic error of the measurements.

Finally, we can use the diffusive motion of the handle beads in the traps during the passive experiments to ensure that the determined PSD of the probe bead is not simply reflecting the fluctuations of the whole cell. Supplementary Fig. 9(a) shows the PSD of the probe bead and the handle beads in the passive experiments (0.1 mW on the probe bead), whereas panel (b) gives the time evolution of these motions. The fluctuations of the free probe bead are significantly larger, which confirms that we can use it to infer information about the cell membrane fluctuations.

QPD and force calibration. For the correct measurement of both the bead motion and the forces applied to the bead, calibration of the QPD as well as the force calibration are key elements. These calibrations are done *in situ* on the beads attached to the cells. QPD calibration is obtained by a rapid scanning protocol that ensures no relevant bead motion during the scan (Supplementary Fig. 10) and by an *in situ* force calibration (Supplementary Methods and Supplementary Fig. 9). As presented in Supplementary Fig. 11, the presence of the cell does influence the position calibration by about 10%. This also leads to a change in trap stiffness in the situation where the cell is attached to the beads (Supplementary Methods for details). Both effects are accounted for in the *in situ* calibration. It should be noted that force calibration is possible even in the absence of a priori knowledge concerning the friction in the cell-bead system. The *in situ* calibration strategy also becomes important when the cells change their shape—for example under ATP-depletion, where the procedure used ensures a correct interpretation of the measurements. As the QPD calibration depends on a precise interpretation of the QPD signal on rapid laser motion, artefacts from the repositioning of the laser are suppressed by exclusively taking the data acquired during the time the laser rests at a given position (Supplementary Fig. 12).

More details about the scanning routines, force calibration and the experimental procedure can be found in the Supplementary Methods.

References

66. Pierrat, S., Brochard-Wyart, F. & Nassoy, P. Enforced detachment of red blood cells adhering to surfaces: statics and dynamics. *Biophys. J.* **87**, 2855–2869 (2004).